Journal of Power Sources 222 (2013) 498–502

Contents lists available at SciVerse ScienceDirect

Journal of Power Sources

journal homepage: www.elsevier.com/locate/jpowsour

Short communication

Carbon nanoporous layer for reaction location management and performance enhancement in all-vanadium redox flow batteries

M.P. Manahan [a], Q.H. Liu [b], M.L. Gross [c], M.M. Mench [b,d,*]

[a] Department of Mechanical and Nuclear Engineering, The Pennsylvania State University, University Park, PA 16802, USA
[b] Electrochemical Energy Storage and Conversion Laboratory, Department of Mechanical, Aerospace, and Biomedical Engineering, The University of Tennessee, Knoxville, TN 37996, USA
[c] Department of Materials Science and Engineering, The Pennsylvania State University, University Park, PA 16802, USA
[d] Energy and Transportation Science Division, Oak Ridge National Laboratory, Oak Ridge, TN 37831, USA

HIGHLIGHTS

- A thin layer of CNTs was added to all-vanadium redox flow battery electrodes.
- This is the first time a separate layer of carbon nanotubes has been used in VRFBs.
- The CNT layer was used to locate where reactions are most favorable within the cell.
- Performance increased with the CNT layer near the negative electrode flow field.

ARTICLE INFO

Article history:
Received 31 July 2012
Received in revised form
30 August 2012
Accepted 31 August 2012
Available online 10 September 2012

Keywords:
All-vanadium redox flow batteries
Polarization
Carbon paper
Reaction location
Carbon nanotube

ABSTRACT

In this study, the performance and reaction location in a VRFB was investigated with a carbon paper electrode that was modified to include a thin layer of multi-walled carbon nanotubes. The nanotube layer was introduced into the electrode at locations on the negative and positive electrode nearest the membrane and nearest the flow field. Results with the nanotube layer on the positive electrode yielded small changes in the performance, despite the location. However, when the nanotube layer was introduced on the negative electrode, the performance was greatly improved when it was closest to the current collector. In this configuration, an 8% increase in power density and a 65 mV increase in cell voltage were observed, compared to a cell with raw carbon paper. This is attributed to the increase in active area of the nanoporous structure in a location where the reaction is favored to occur.

Published by Elsevier B.V.

1. Introduction

The all-vanadium redox flow battery (VRFB) has been under significant development for grid leveling and renewable energy conversion and storage applications [1]. VRFB systems contain a negative and a positive half-cell where four oxidation states of V^{2+}/V^{3+} and V^{4+}/V^{5+} (present as VO^{2+}/VO_2^+) serve as redox couples at the respective electrodes, as shown in Eqs. (1) and (2):

$$V^{3+} + e^- \underset{\text{discharge}}{\overset{\text{charge}}{\rightleftharpoons}} V^{2+}, \quad E^0 = -0.26 \text{ V vs. NHE} \tag{1}$$

$$VO^{2+} + H_2O \underset{\text{discharge}}{\overset{\text{charge}}{\rightleftharpoons}} VO_2^+ + 2H^+ + e^-, \; E^0 = 1.00 \text{ V vs. NHE} \tag{2}$$

Carbon-based porous materials have been widely used as electrodes on both the negative and positive half-cells. Carbon felt materials have been typically employed [2,3], however recent studies have shown that carbon paper (CP) can yield significantly enhanced performance [4,5], although possible degradation issues are not yet not fully understood or resolved. In particular, Refs. [4,5] show a maximum power density of more than five times other published levels at 60–100% state of charge range.

* Corresponding author. Electrochemical Energy Storage and Conversion Laboratory, Department of Mechanical, Aerospace, and Biomedical Engineering, The University of Tennessee, Knoxville, TN 37996, USA. Tel.: +1 865 974 6751; fax: +1 865 974 5274.
E-mail addresses: matthewmench@gmail.com, mmench@utk.edu (M.M. Mench).

0378-7753/$ – see front matter Published by Elsevier B.V.
http://dx.doi.org/10.1016/j.jpowsour.2012.08.097

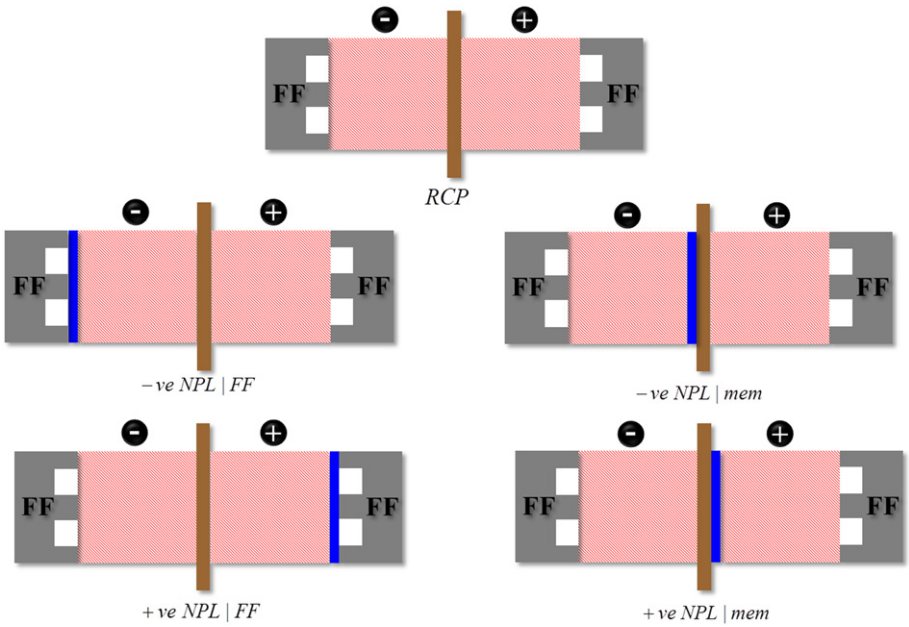

Fig. 1. A schematic of the nanoporous layer (NPL) orientations tested. The solid blue region represents the NPL, the hashed region represents carbon paper, the brown separator represents the membrane (mem), and the flow field (FF) is as labeled (not to scale). (For interpretation of the references to colour in this figure legend, the reader is referred to the web version of this article.)

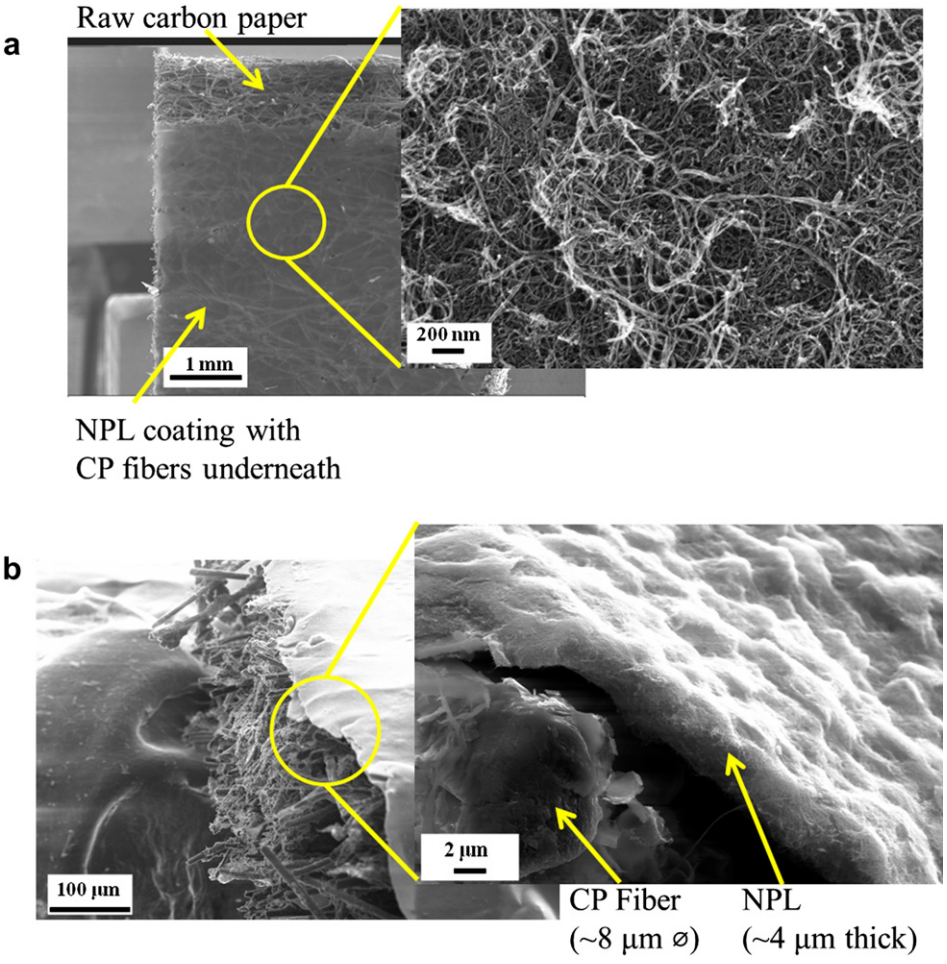

Fig. 2. (a) Top-down SEM image of CP with NPL coating and a close-up of the NPL. (b) Angled view of CP with NPL and close-up of a CP fiber and NPL.

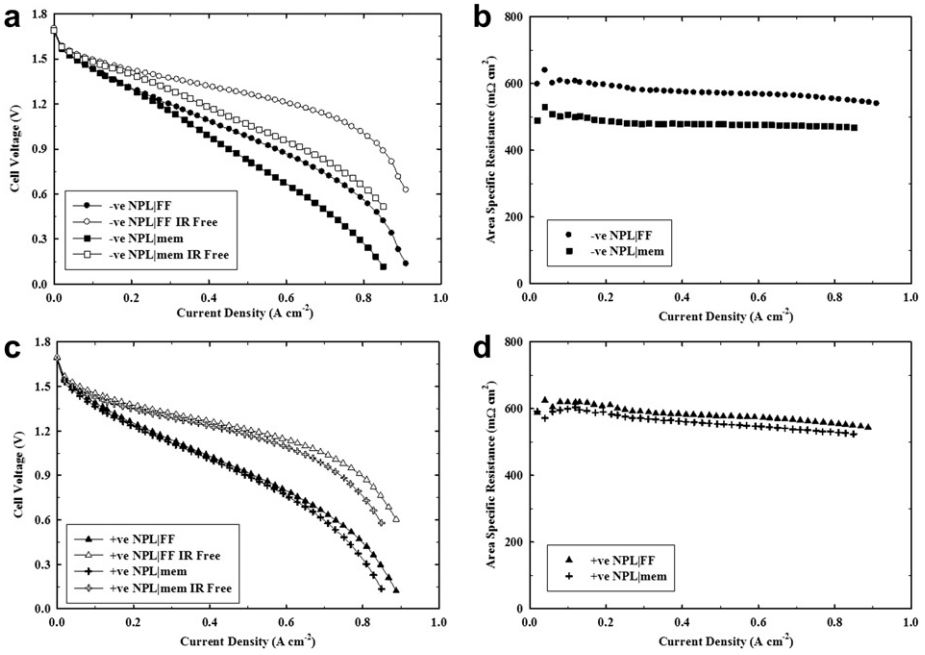

Fig. 3. Polarization curves and ASR plots of the negative electrodes ((a) and (b), respectively), and the positive electrodes ((c) and (d), respectively) for the NPL facing the flow field (FF) and the membrane (mem).

Presently, multi-walled carbon nanotubes (MWCNTs) have been explored for multiple energy applications and shown to be potentially useful candidates in areas such as organic photovoltaics, fuel cell catalyst support, and various electrodes [6–9]. Recently, two studies have investigated the introduction of carbon nanotubes (CNTs) into the VRFB electrodes [10,11]. Zhu et al. [10] mixed CNTs with graphite and observed an increase in the peak current of cyclic voltammograms, which they ascribed to increased active surface area. Li et al. [11] found that hydroxyl- and carboxyl-functionalized MWCNTs are beneficial to VRFB performance.

In this work, a customizable and separate layer of MWCNTs, referred to as the nanoporous layer (NPL), is applied as an additional layer onto CP and is placed at different locations in the cell to test its effect on polarization behavior [12] and help understand the location of limiting electrochemical reaction in the redox cell. To the authors' knowledge, this is the first experiment with a discrete CNT layer for VRFB electrodes. Although not explicitly investigated herein, the NPL holds the ability in principle to be custom-modified by tailoring the porosity [13], surface functional groups [11,14], and thickness.

2. Experimental

Carbon paper type SIGRACET SGL 10 AA from SGL Group (Germany) was used as-received. MWCNTs from CheapTubes, Inc. (USA) were purified by a method described by O'Connell, et al. [15]. Briefly, MWCNTs were sonicated in distilled water with 1 wt% ultra-pure sodium dodecyl sulfate (SDS) surfactant (MP Biomedicals, USA). The SDS-MWCNT solution was centrifuged at ~12,000*g* for 4 h. To produce the NPL, the Wu et al. [16] method (membrane filtration of the supernatant) was adopted. The samples were thoroughly rinsed with distilled water and dried at room temperature before use.

A Fuel Cell Technologies (USA) 5-cm^2, single-serpentine flow channel cell and Nafion 117 membrane were used for testing. As the standard electrode, one layer of SGL 10 AA raw carbon paper (RCP) was used as the negative and positive electrode. The NPL was made to be sufficiently thin (~4 μm, <1% of RCP uncompressed thickness) and was placed in four orientations in the cell: (i & ii) NPL toward the flow field (FF) and toward the membrane on the negative electrode ("−ve NPL|FF" and "−ve NPL|mem", respectively), and (iii & iv) NPL toward the flow field (FF) and toward the membrane on the positive electrode ("+ve NPL|FF" and "+ve NPL|mem"). A schematic of these orientations is shown in Fig. 1.

The initial batch of electrolyte (1 mol L^{-1} $VOSO_4$ + 5 mol L^{-1} H_2SO_4) was initially charged in two steps: (i) constant current of 0.5 A until a cell potential of 1.8 V was achieved, then (ii) constant potential of 1.8 V until the current was less than 5 mA. Discharge polarization data were collected galvanostatically at room temperature, stepping current by 0.1 A increments using a Scribner Associates (USA) 857 redox cell test system. Additionally, at least five polarization curves were obtained for each cell to ensure stability and repeatability. Flow rates were held constant at 90 mL min^{-1}, which corresponds to a stoichiometry of greater than

Table 1
Summary of performance characteristics for each tested electrode configuration.

Electrode configuration	OCV (mV)	Average ASR (mΩ cm^2)	Limiting current density (mA cm^{-2})	Voltage drop at 20 mA cm^{-2} (mV)	Peak power density (mW cm^{-2})	State of charge at peak power (%)
RCP	1.71	604	909	153	483	70
−ve NPL|FF	1.70	576	910	117	524	68
−ve NPL|mem	1.69	483	851	121	413	80
+ve NPL|FF	1.70	583	888	145	478	70
+ve NPL|mem	1.68	561	849	152	461	72

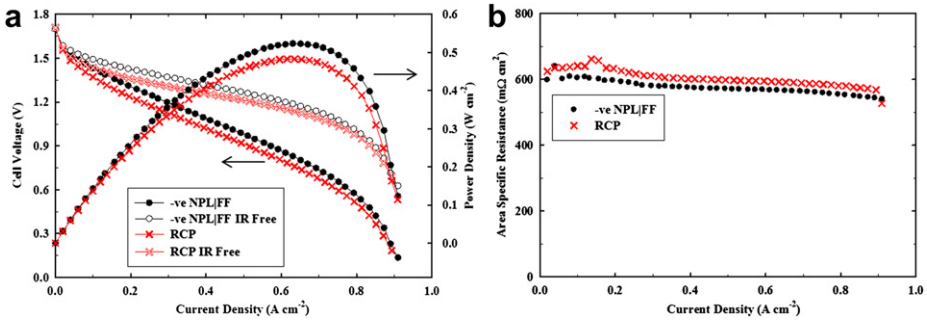

Fig. 4. (a) Polarization and power curves and (b) ASR of the −ve NPL|FF compared to the RCP.

31 at the highest limiting current obtained. The negative electrolyte compartment was purged with nitrogen to avoid oxygen interaction. The errors in polarization data we can attribute to build-to-build variation were measured and determined to be between 2.5 and 5% over the current range tested.

3. Results and discussion

3.1. Morphology and characterization of NPL electrode materials

Fig. 2 shows SEM images of the RCP and NPL. It is evident the surface roughness of the NPL is much lower than the course-fibered RCP. The NPL-CP composite remained intact via Van der Waals forces as well as physical comingling resulting from contact between the MWCNTs and the CP fibers. While the NPL remained adhered to the CP during experimentation, there was some detachment upon disassembling the cell, indicating the need for better adhesion in future applications. Finally, the contact angle of electrolyte solution was measured for both the NPL (∼136°) and the RCP (∼132°), indicating the two surfaces to have similar wettability characteristics.

3.2. Effect of NPL orientation on performance

Fig. 3 compares the performance characteristics of the NPL|FF and NPL|mem on the negative electrode (Fig. 3a, b) and on the positive electrode (Fig. 3c, d). Fig. 3a shows a similar kinetic region for both NPL orientations on the negative electrode; however increased polarization is observed for the −ve NPL|mem orientation at currents higher than ∼0.2 A cm^{-2}, and the limiting current is reduced by about 7% compared to −ve NPL|FF. The reduction in limiting current of the −ve NPL|mem indicates higher mass-transport related polarization compared to the *−ve NPL|FF*. The area-specific resistance (ASR) data (Fig. 3b) shows the −ve NPL|mem has approximately 100 mΩ cm^2 lower resistance than the −ve NPL|FF. Although there is some ohmic benefit of the −ve NPL|mem, the mass-transport related losses dominate and lead to reduced overall performance. These effects are suspected to arise due to the pore-size differences between the CP and NPL and hindered charged species transport from the membrane to the reaction location.

On the positive electrode (Fig. 3c, d), the +ve NPL|FF exhibited slightly increased performance compared to the +ve NPL|mem, and both orientations yield approximately the same ASR. Comparing the performance of all orientations in Fig. 3, the −ve NPL|FF displays the best performance of all the single-NPL orientations (see also Table 1).

These results give insight into questions regarding where the majority of the electrochemical reactions happen. The performance benefits observed with −ve NPL|FF can be a result of placing a high active surface area material (the NPL) near where the electrochemical reaction is most favorable (near the flow field). This conclusion is consistent with the modeling and experimental results from Refs. [5,17]. Finally, Fig. 4a shows the −ve NPL|FF orientation has 8% increased power density compared to RCP along with approximately 65 mV increased voltage across most of the current range. Losses related to the ASR (Fig. 4b) account for only ∼15 mV of the voltage difference, suggesting the −ve NPL|FF improves the electrode kinetics. This also indicates the negative electrode kinetics are limiting under these discharge conditions compared to the positive electrode. Near the limiting current, however, the −ve NPL|FF displays increase mass-transport losses, likely resulting from flow/transport inhibition due to the nanoscale pore structure of the NPL. Table 1 summarizes the key performance results of all the experiments.

4. Conclusions

This study shows the promise of incorporating stand-alone nanoporous layers into all-vanadium redox flow battery design. A layer of MWCNTs, named the nanoporous layer (NPL), was coated onto one side of raw carbon paper and utilized to study the impact on performance and understand some details on the reaction location and relative dominance of the electrode kinetics. An NPL was placed in different locations in the cell: on the negative and positive electrodes in contact with either the flow field or the membrane. When the NPL was located on the negative electrode toward the flow field, an 8% increase in power density and a 65 mV increase in cell voltage were observed compared to a cell with raw carbon paper. Because 40 mV of the increase could not be attributed to ohmic losses, the primary suspected cause for the improvement is the increase in active surface area of the nanoporous structure of the NPL in a location where the reaction is favorable to occur (toward the flow field). Finally, it is suggested that the pore and surface structure of the NPL can be customized to minimize mass-transport losses while providing a high surface area electrode for improved performance over current state-of-the-art materials.

Acknowledgments

M.P. Manahan acknowledges the National Science Foundation Graduate Research Fellowship Program (NSF GRFP) #DGE-0750756 and M.M. Mench thanks the NSF #CBET-0644811 for partial support of this work.

References

[1] A. Weber, M.M. Mench, J. Meyers, P. Ross, J. Gostick, Q. Liu, Journal of Applied Electrochemistry 41 (2011) 1137–1164.

[2] B. Sun, M. Skyllas-Kazacos, Electrochimica Acta 37 (1992) 1253–1260.
[3] B. Sun, M. Skyllas-Kazacos, Electrochimica Acta 37 (1992) 2459–2465.
[4] D.S. Aaron, Q. Liu, Z. Tang, G.M. Grim, A.B. Papandrew, A. Turhan, T.A. Zawodzinski, M.M. Mench, Journal of Power Sources 206 (2012) 450–453.
[5] Q.H. Liu, G.M. Grim, A.B. Papandrew, A. Turhan, T.A. Zawodzinski, M.M. Mench, Journal of Electrochemical Society 159 (2012) A1246–A1252.
[6] E. Kymakis, G.A.J. Amaratunga, Applied Physics Letters 80 (2002) 112–114.
[7] L. Hu, J.W. Choi, Y. Yang, S. Jeong, F. La Mantia, L.-F. Cui, Y. Cui, Proceedings of the National Academy of Sciences 106 (2009) 21490–21494.
[8] Z. Liu, X. Lin, J.Y. Lee, W. Zhang, M. Han, L.M. Gan, Langmuir 18 (2002) 4054–4060.
[9] M.L. Gross, K.R. Zavadil, M.A. Hickner, Journal of Material Chemistry 21 (2011) 14259–14264.
[10] H.Q. Zhu, Y.M. Zhang, L. Yue, W.S. Li, G.L. Li, D. Shu, H.Y. Chen, Journal of Power Sources 184 (2008) 637–640.
[11] W. Li, J. Liu, C. Yan, Carbon 49 (2011) 3463–3470.
[12] D. Aaron, Z. Tang, A. Papandrew, T. Zawodzinski, Journal of Applied Electrochemistry 41 (2011) 1175–1182.
[13] R.L.D. Whitby, T. Fukuda, T. Maekawa, S.L. James, S.V. Mikhalovsky, Carbon 46 (2008) 949–956.
[14] J.L. Bahr, J. Yang, D.V. Kosynkin, M.J. Bronikowski, R.E. Smalley, J.M. Tour, Journal of American Chemical Society 123 (2001) 6536–6542.
[15] M.J. O'Connell, S.M. Bachilo, C.B. Huffman, V.C. Moore, M.S. Strano, E.H. Haroz, K.L. Rialon, P.J. Boul, W.H. Noon, C. Kittrell, J. Ma, R.H. Hauge, R.B. Weisman, R.E. Smalley, Science 297 (2002) 593–596.
[16] Z. Wu, Z. Chen, X. Du, J.M. Logan, J. Sippel, M. Nikolou, K. Kamaras, J.R. Reynolds, D.B. Tanner, A.F. Hebard, A.G. Rinzler, Science 305 (2004) 1273–1276.
[17] D. You, H. Zhang, J. Chen, Electrochimica Acta 54 (2009) 6827–6836.